HHS Public Access

Author manuscript

Lab Invest. Author manuscript; available in PMC 2021 November 20.

Published in final edited form as:

Lab Invest. 2021 September ; 101(9): 1186–1196. doi:10.1038/s41374-021-00609-2.

Quantitative 3-dimensional imaging and tissue cytometry reveals lymphatic expansion in acute kidney injury

Laurence M. Black[1,2], **Seth Winfree**[3,4,5], **Suraj D. Khochare**[3,4,5], **Malgorzata M. Kamocka**[3,4,5], **Amie M. Traylor**[1,2], **Stephanie K. Esman**[1,2], **Shehnaz Khan**[3,4,5], **Abolfazl Zarjou**[1,2], **Anupam Agarwal**[1,2,7], **Tarek M. El-Achkar**[3,4,5,6]

[1]Department of Medicine, University of Alabama at Birmingham, Birmingham, AL, 35294, USA

[2]Nephrology Research and Training Center, University of Alabama at Birmingham, Birmingham, AL, 35294, USA

[3]Indiana University School of Medicine, Department of Medicine, Division of Nephrology, Indianapolis, IN 46202, USA

[4]Indiana University School of Medicine, Department of Cellular & Integrative Physiology, Indianapolis, IN 46202, USA

[5]Indiana Center for Biological Microscopy, Indianapolis, Indiana, 950 W. Walnut Street, Indianapolis, IN 46202, USA

[6]Indianapolis Veterans Affairs Medical Center, Indianapolis, Indiana, USA

[7]Department of Veterans Affairs, Birmingham, AL, USA

Abstract

The lymphatic system plays an integral role in physiology and has recently been identified as a key player in disease progression. Tissue injury stimulates lymphatic expansion, or lymphangiogenesis (LA), though its precise role in disease processes remains unclear. LA is associated with inflammation, which is a key component of acute kidney injury (AKI), for which there are no approved therapies. While LA research has gained traction in the last decade, there exists a significant lack of understanding of this process in the kidney. Though innovative studies have elucidated markers and models with which to study LA, the field is still evolving with ways to visualize lymphatics *in vivo*. Prospero-related homeobox-1 (Prox-1) is the master regulator of LA and determines lymphatic cell fate through its action on vascular endothelial growth

Corresponding authors: Tarek M. El-Achkar, MD, Division of Nephrology, Indiana University, Indianapolis, IN 46202, telachka@iu.edu; Anupam Agarwal, MD, Division of Nephrology, University of Alabama at Birmingham, Birmingham, AL 35294, agarwal@uab.edu.

Author Contributions

LMB, AMT, AZ, AA, and TME-A designed studies. LMB, SW, SDK MK, AMT, SKE, and SK conducted experiments. LMB, SW, SDK MK, AMT, SKE, and SK acquired data. LMB, SW, and SDK analyzed data. LMB, SW, SDK, and TME-A interpreted data. LMB, SW, SDK, MK, AMT, and SKE provided methodology expertise. AA and TME-A provided reagents and resources. LMB, AA, and TME-A wrote the manuscript. All authors reviewed, edited, and approved the final version of the manuscript.

Disclosures

AA serves as a consultant for Dynamed and is on the advisory boards of Goldilocks Therapeutics, Alpha Young and Angion for work outside the scope of this manuscript.

factor receptor expression. Here, we investigate the consequences of AKI on the abundance and distribution of lymphatic endothelial cells using Prox1-tdTomato reporter mice (ProxTom) coupled with large-scale three-dimensional quantitative imaging and tissue cytometry (3DTC). Using these technologies, we describe the spatial dynamics of lymphatic vasculature in quiescence and post-AKI. We also describe the use of lymphatic vessel endothelial hyaluronan receptor-1 (LYVE-1) as a marker of lymphatic vessels using 3DTC in the absence of the ProxTom reporter mice as an alternative approach. The use of 3DTC for lymphatic research presents a new avenue with which to study the origin and distribution of renal lymphatic vessels. These findings will enhance our understanding of renal lymphatic function during injury and could inform the development of novel therapeutics for intervention in AKI.

Keywords

lymphatics; kidney; inflammation; lymphangiogenesis; imaging

Introduction

The lymphatic system, found intertwined with the blood vasculature, is essential for fluid and electrolyte homeostasis, immune surveillance, and lipid and cholesterol transport[1]. Lymph vessels are found in nearly every vascularized tissue, and are controlled by tightly regulated signaling pathways[2,3]. Lymphatic vessel failure exacerbates disease processes and leads to fluid retention and dysfunctional immune response[3], making it a significant effector of disease progression. Lymphatic vessel formation, or lymphangiogenesis (LA), primarily occurs in development; however, LA also occurs as a consequence of organ injury[4-9].

The lymphatic system was first described between the 5th to 3rd century BC[10,11]; however, these structures were only identified by their morphology until the late 1990s when vascular endothelial growth factor (VEGF-C) and its receptor, VEGF-R3, were described to drive hyperplasia of the lymphatic vasculature[12]. Since then, the molecular basis of LA has continued to be explored[10,13]. In the kidney, lymphatic vessels are present in quiescence mainly in the hilum and cortex, and less so in the medulla, with intralobular lymphatics interlaced with the renal arteries and arterioles[14]. These structures are reliably identifiable by their expression of the master transcription factor Prospero homeobox protein 1 (Prox-1) and lymphatic vessel hyaluronan receptor-1 (LYVE-1), as well as membrane glycoprotein podoplanin and VEGFR-3.

While the precise function of the renal lymphatic system has yet to be fully elucidated[15], we and others have described renal LA to occur as a response to kidney injury[5,6,16,17]; however there exists conflicting reports in various rodent models about whether pro- and anti-lymphangiogenic factors exacerbate renal injury. It is imperative that work in the field of renal LA focus on fully understanding the contextual contribution of LA to the pathogenesis of acute kidney injury (AKI) by assessing the spatial and molecular dynamics of this process.

Due to the fact that lymphatic vessels are difficult to visualize *in vivo*, Truman and colleagues developed a mouse that expresses red fluorescent protein tdTomato under the

direction of the Prox-1 promoter (ProxTom)[18]. These mice provide high visibility of Prox-1-positive cells endogenously, without the need for exogenous methods such as tracer dye injections or co-staining. These mice show unique promise to advancing the field of lymphatic biology due to their specificity and reliability; however, their use has not been explored in the context of kidney disease.

Visualizing clear lymphatic vessels requires either antibody staining for immunohistochemical applications or tracer absorption and downstream imaging such as lymphoscintigraphy, positron emission tomography (PET) or computed tomography (CT). Furthermore, due to the complexity of studying lymphatic vasculature, as it twists and plunges deep within the tissue, standard imaging techniques make it challenging to accurately understand the spatial location of renal lymphatics. To this end, we have established a method to visualize LA post-AKI using large scale three-dimensional (3D) imaging and tissue cytometry (3DTC)[19-21]. This technique has recently emerged at the forefront of precision medicine and allows for high-resolution imaging at the subcellular level of entire tissue sections with mesoscale dimensions[22], making it ideal to characterize the abundance, spatial distribution, and structural significance of lymphatics in the kidney.

Using multiple models of kidney injury, we recently demonstrated a robust and dynamic induction of renal LA regardless of initial insult[1]. We described lymphangiogenic ligands, VEGF-C and -D, to be abundant in the tubules in quiescence. After injury, their tubular expression was altered and VEGF-C and -D became detectable in the urine and serum. Renal tubules are at least in part responsible for LA signaling during injury and are involved in secretion of these factors into the interstitium and lumen. As a response to this signaling, we observed LA in AKI as demonstrated by increased abundance of VEGFR-3 positive vessels[1].

To further elucidate the complexities of lymphatic vessels during kidney injury, here we aim to characterize the use of 3DTC as a novel method with which to investigate lymphatic vessels during injury to better understand spatial characteristics and functional significance. In this study, we utilize novel ProxTom mice to visualize LA post-AKI with high sensitivity and minimal manipulation ex-vivo using 3DTC. Using these methods, new avenues that explore spatial dynamics and cell communication emerge to further LA-specific pathways and lymphatic vessel function to allow for the development of therapeutic targets for AKI.

Materials and Methods

Animals.

Mice were obtained from The Jackson Laboratory (B6;129S-Tg(Prox1-tdTomato)12Nrud/J; Stock No: 018128l and C57BL/5J; Stock No: 000664). Male mice aged 10-12 weeks were used for these studies. The genotype of transgenic mice was confirmed by PCR analysis on genomic DNA obtained from the tail, as previously described[18]. Bilateral ischemia-reperfusion injury (IRI; 20 minutes) was performed on mice to induce AKI as previously reported[23].

Tissue processing for 3-dimensional (3D) imaging and tissue cytometry (3DTC).

Mice were anesthetized with isoflurane (2.5% v/v induction, 1.5% v/v maintenance) and perfused with 10 ml cold phosphate buffered saline (PBS) through the left ventricle. Kidneys were fixed in 4% paraformaldehyde (PFA) and subsequently transferred to 0.25% PFA in PBS. 50 micron sections were cut on vibratome (Leica) and stained with 4′,6-diamidino-2-phenylindole (DAPI) and Oregon Green Phalloidin[24,25] and mounted in Prolong Glass (ThermoFisher) and cured for 4 days before sealing.

Large scale 3D imaging.

Mounted sections were imaged *in toto* on a Leica SP8 with 4 channel sequential acquisition mode (Blue – 405 nm excitation, 420-490 nm emission, Green – 488 nm excitation, 500-550 nm emission, Orange – 552 nm excitation, 560-630 nm emission and Deep red – 638 nm excitation, 650-750 nm emission) with a HC PL APO 20X/0.75 IMM objective using Leica immersion oil RI=1.51. Volumetric tile scanning of the entire section was performed overnight (10-14 hours imaging/section) and the image volumes were digitally stitched using Leica LASX software. The same microscope settings were used to image all the sections studies. The resulting 4 channel large scale volumes (40-50 GB, .lif file formats) were copied to a dedicated storage server for processing and analysis.

Image preprocessing and analytics.

The data was converted from 16 to 8 bits and underwent noise reduction in all channels with a 3D median filter (kernel size of 1.0) using ImageJ. This filtered data was loaded into Volumetric Tissue Exploration and Analysis (VTEA) for further processing and analysis. A computer dedicated for image analytics (256GB RAM, Intel Xeon CPU with 2x Nvidia RTX 2080Tis) was used. Segmentation and analysis were performed in v.1.0-alpha of VTEA (https://github.com/icbm-iupui/volumetric-tissue-exploration-analysis). VTEA's LS Connect3D (Large Scale Connect 3D), a region based connected components segmentation, was used for nuclear segmentation. To assign cell type, intensity was measured in the accompanying channels within these nuclei and within a fixed distance away from these nuclei- a 3D morphological grow routine. The settings and parameters for segmentation were consistent indicating adequate staining and quality of the nuclei. Briefly, minimum intensity (“Low Threshold”) was calculated by ImageJ from the nuclear channel image (IJ_Isodata, https://imagej.net/Auto_Threshold#Default), and the default LS Connect3D settings of distance (“Centroid Offset” = 5) and segmented object size (“Min Vol (vox)” = 20; “Max Vol (vox)” = 1000).

VTEA analysis.

Fluorescence from td-Tomato (indicating Prox1 promoter activity) associated with nuclei by the 3D morphological grow routine described above were displayed on a scatterplot as individual points. All analyses include 1) a segmentation preview described above, 2) a .csv file with all segmented and measured "nuclei"/cells, 3) an .obx file that contains the segmented nuclei for future analysis with associated and coded image file, 4) gates for loading into VTEA (.vtg files), 5) an image of the plot(s) as a png file, 6) pertinent ImageJ ROIs and 7) composite images with gated cells indicated for rendering and presentation.

Direct visualization of the gated cells on the image allows validation of the gates, which was performed individually on random fields for each large-scale image volume. The dimensions of the tissue within the image volumes were calculated using ImageJ region-of-interest tools.

LYVE-1 staining and imaging.

50 micron kidney sections from quiescent C57Bl/6 mice were processed as described above were stained with DAPI, Phalloidin and LYVE-1 using anti-LYVE-1 polyclonal antibody (Novus Biologicals, NB600-1008). After mounting on glass slides, stained sections were viewed under Olympus FluoView laser-scanning confocal microscope[26]. Tissue cytometry was performed using VTEA and visualization of gated cells using 3D rendering was accomplished with ClearVolume[27].

Von Willebrand Factor (VWF) staining and imaging.

Staining for VWF was performed using anti-VWF antibody (Novus Biologicals, NB600-586) on kidney sections from mice after IRI or control as described above. Large scale imaging and digital stitching were performed using the Leica SP8 and Leica LASX software as discussed above.

3D rendering and videos of large-scale image volumes.

The animations of the volume rendering for the data shown in video 1 and video 2 were generated using Imaris Software (Version 8.1.2, Oxford Instruments, Concord, MA)[25] and normal shading volume rendering mode. Prox-1 channel was processed with Imaris Channel Arithmetics function to subtract background fluorescence signal sourced from erythrocytes and captured in “deep red” channel. Surface segmentation was used to mask the Prox-1 channel and eliminate an additional strong background fluorescence detected in injured kidneys. 3D rendering of video 3 was done using ClearVolume[27].

Image processing for figures.

Quantitative analysis was conducted using raw image data, but micrograph images presented in figures were contrast enhanced in a way that preserved the visibility of both the dim and bright structures of the original images. Images in figures were processed, assembled and annotated using Adobe Photoshop.

Statistics.

Data are represented as mean ± SEM. A two-tailed t-test was used to compare the abundance and density of Prox1 cells between injury and controls groups. Statistical significance was defined as $p<0.05$.

Results

VTEA analysis methods to parse autofluorescence (AF) post-AKI.

To interrogate LA post-AKI with 3DTC, mice underwent 20 minutes of bilateral renal ischemia, followed by reperfusion (IRI). Kidneys were collected at day 3 post-IRI for image processing. AKI causes significant trauma to the kidneys, leading to necrotic tubules,

basement membrane detachment, loss of brush border, tubular casts, and accumulation of cellular debris[28]. To this end, one of the major challenges that we addressed when performing large scale 3D imaging and tissue cytometry was the AF signal in the red channel that increased after IRI, due to factors such as cell debris, injury, and cast formation. To separate AF from the true tdTomato signal, we collected photons in the far-red channel, which is solely from the endogenous tissue fluorescence.

We hypothesized that endogenous fluorescence post-injury would have a broad emission spectrum, which would encompass the red and far-red spectra. We therefore used the far-red signal as a surrogate of AF to parse out td-Tomato signal from the endogenous red fluorescence and to develop a gating strategy (Figure 1). This strategy was tested and validated using negative control (td-Tomato$^-$) IRI specimen, whereby we did not observe any significant signal in the red gate.

Prox-1 signal following AKI suggests lymphatic expansion.

We have previously characterized LA post-AKI and described lymphatic vessel proliferation, regardless of injury model[1], which we were able to demonstrate using 3DTC in this work. IRI kidneys displayed a significant increase in Prox-1$^+$ cells compared to baseline (Figure 2). Analysis revealed significantly increased cells per section in the IRI samples versus baseline (667.0 ± 121.6 vs. 156.0 ± 58 Prox-1$^+$ cells per section, $p<0.05$) and we observed significantly higher density of Prox-1$^+$ cells per mm^3 (717.2 ± 161.8 vs. 174.4 ± 62.1 Prox-1$^+$ cells/mm^3, $p<0.05$). Additionally, 0.19% of total segmented cells were identified as Prox-1$^+$ post-IRI, compared to 0.05% in the baseline kidneys ($p = 0.06$). The results from each sample is shown in Table 1, with the total number of Prox-1$^+$ cells identified in each section, the percentage of the total number of segmented cells, and the density of Prox-1$^+$ cells in each sample. Herein, VTEA analysis confirms our previous findings that LA and lymphatic vessel expansion occurs post-AKI.

Distribution of Prox-1 cells is altered post-AKI.

Kidney sections were stained with DAPI (nuclei) and F actin (filamentous actin), in addition to the endogenous Prox1-tdTomato label, and imaged with 3D confocal microscopy (Leica SP8). We were able to reliably detect robust Prox1-tdTomato signal in baseline control kidneys with variability. Quiescent signal was predominately localized to the renal hilum and around large vessels, consistent with what is expected of lymphatic distribution (Video 1). The distribution of Prox-1$^+$ cells following IRI is different than that of baseline, with Prox-1$^+$ cells predominately localized to the inner stripe of the outer medulla, with small expansion in the lower outer stripe of the outer medulla near the injured S3 segment, in contrast to hilar localization near large vessels (Figure 3, Video 2).

IRI requires the physical clamping of the renal artery and vein, which damages the vasculature and may augment angiogenesis. Additionally, the ischemic injury stimulates angiogenic factor expression[29]. Though Prox-1 expression is predominantly localized to lymphatic endothelial cells, it has been reported that the vasa recta is a “lymphatic-like vessel” that atypically expresses Prox-1 and VEGFR-3[30]. To account for injury-induced expansion of the blood vasculature, including Prox-1$^+$ vasa recta, we stained quiescent and

injured kidney sections with von Willebrand Factor (VWF)[31]. The observed distribution of VWF staining was predominately in the glomeruli, cortical peritubular capillaries, and vasa recta in the deep inner medulla and papilla in the quiescent state (Figure 4A-C). After IRI, there was a variable increase in VWF signal. Importantly, the distribution of the increase is different than the observed Prox-1 signal. VWF^+ cells were localized to the outer stripe region, contiguous with the corticomedullary junction (Figure 4D), in contrast to the $Prox\text{-}1^+$ cells which were localized in the inner stripe of the outer medulla, further distinguishing the changes between lymphatic and blood vasculature.

LYVE-1 as alternative lymphatic marker for VTEA analysis.

ProxTom mice are ideal for studying lymphatic development and LA due to the endogenous red fluorescent protein that is under the control of the Prox-1 promoter, which is the master regulator of LA[18]. One limitation to the use of these mice is that most hemizygous males are sterile; therefore, hemizygous females must be bred with wild-type male mice. Furthermore, these mice were generated on a C57BL/6 background[18] and we observe that this line has small litter sizes, which makes it difficult to produce enough mice for timely experiments. To overcome this, it is suggested to cross ProxTom females with B6129SF1/J mice (Jackson Labs).

LYVE-1 is a surface receptor which aids in the metabolism of lymph hyaluronan, a major responsibility of the lymphatic system[32]. Regarded for its specificity and widespread use as a lymphatic marker, LYVE-1 has a similar expression pattern to Prox-1, though LYVE-1 is also expressed by macrophages[18,33,34]. To overcome the limitations presented by the ProxTom mice, we have optimized the use of wild-type mice for 3DTC to study LA by staining quiescent kidney sections with LYVE-1 antibody. Wild-type kidneys were collected and stained with DAPI, F-Actin, and LYVE-1 antibody and processed for imaging. We demonstrate robust $LYVE\text{-}1^+$ staining specific to lymphatic vessels (Figure 4, Video 3) and validate this staining method as a viable alternative for ProxTom mice.

Discussion

Our goal was to validate techniques to study renal LA after injury, an area that is poorly understood. We demonstrated that the novel use of ProxTom mice coupled with 3DTC as a reliable tool to study this process in the kidney. ProxTom mice allow for direct imaging of lymphatic vasculature, which is an advantage for large scale imaging. These reporter mice elicit a robust and dependable tdTomato signal that has implications for a number of other techniques, such as flow cytometry.

LA is observed in various kidney diseases, such as IgA nephropathy, diabetic kidney disease, chronic kidney disease, lupus nephritis, focal glomerulosclerosis, among others; however, the function of this process is not well understood[35]. We have previously demonstrated renal LA to occur as a response to models of AKI and CKD, with signaling seemingly originating from tubular epithelial cells, which express large amounts of LA factors, VEGF-C and -D. The LA ligands become detectable in the serum and urine post-AKI, suggesting systemic signaling. As a response to these factors, the renal lymphatic network undergoes massive LA, as shown by increased abundance of VEGFR3-positive vessels[1].

3DTC is a viable avenue with which to study renal lymphatic biology. This technique uses multiplexed fluorescence staining to quantitate spatial position and protein expression of specific cell types without particular biases that originate from tissue digestion and homogenization[20]. Other methods available have significant limitations in regards to studying renal lymphatic architecture, spatial location, and LA in the kidney due to the nature of the vessels embedded within the tissue and their scattered distribution. Without using 3D imaging of the kidney, data regarding such structures is lost when evaluating individual planes. ProxTom mice allow for imaging of highly visible Prox-1$^+$ lymphatic vessels with no external manipulation, implicating their use for a wide range of techniques including *in vivo* imaging, confocal microscopy, 3DTC, and flow cytometry. Using 3DTC, we were able to develop a feasible and reproducible strategy that is able to distinguish autofluorescence generated by tissue injury, swelling, molecular disturbances, and cellular breakdown. Applying this analytical strategy allowed for reliable detection of Prox-1$^+$ cells post-IRI.

To this end, we exposed mice to IRI to induce LA as a result of AKI as previously described[1]. We observed that Prox-1$^+$ cells increase with injury, is consistent, and reached significance in the metrics of average cell number per section and average density ($p<0.05$) and trended in percentage of total cells ($p=0.06$). Using this technique, we have confirmed that lymphatic expansion via LA occurs and is detectable by this method.

Renal lymphatics are characteristically located intertwined with the renal artery and vein. Additionally, lymphatic vessels in quiescence are located within the hilum, cortex and cortico-medullary junction, and are absent in the medulla[36]. In this study, we observed the staining pattern of Prox-1$^+$ lymphatics in quiescence to be consistent with what is expected in the hilum and around large vessels. However, we detected substantial changes in lymphatic distribution after injury. At day 3 post-IRI, mice exhibited Prox-1$^+$ vessels that extended from the hilum to the inner stripe of the outer medulla, less so in the outer stripe of the outer medulla, and minimally in the cortex. Renal lymph is rich with transcription factors, enzymes, solutes, signaling factors, and inflammatory cells. After injury, the renal lymphatics may aid in clearance of debris, fluid and excess inflammatory infiltrate; however, there is still conjecture about their specific role[35].

Renal IRI causes temporary hypoxia, followed by reoxygenation, which causes inflammation and oxidative stress. This mode of injury causes widespread damage to the kidney, including damage to the lymphatic vasculature. We have previously demonstrated that the *de novo* lymphatic growth is not affected by the physical clamping of the renal artery and vein during the IRI surgery[1]. The question arises about the origin of *de novo* lymphatic vessels during LA. It has been suggested that tissue injury results in leaky and damaged lymphatics[37]; thus, it is plausible that LA arises from these injured vessels. Others have proposed that macrophages transdifferentiate into lymphatic vessels during LA[38].

LA occurs regardless of mode of renal injury (IRI, acute cisplatin nephrotoxicity, repeated low dose cisplatin, and diphtheria toxin-induced AKI)[1]; however, we have also demonstrated that different modes of injury display divergent pathogenesis and resulting pathology[39]. For example, IRI elicits a robust inflammatory response with prolonged presence of

polymorphonuclear cells, natural killer cells, and macrophages, followed by infiltration of T cells. In contrast, cisplatin nephrotoxicity causes significant leukopenia. Due to the fact that the inflammatory response and, in particular macrophages, play a significant role in LA[7,38,40-43], it would be interesting to investigate the origin of *de novo* lymphatics in different kidney diseases and specifically parse the origin of renal lymphatics post-AKI, with special emphasis perhaps on mode of injury.

Though ProxTom reporter mice are ideal to study LA using 3DTC due to their reliable, Prox1-promoter driven expression of endogenous red fluorescent protein, there are limitations to their use including small litter sizes. To overcome this, we show that 3DTC can be successfully accomplished using LYVE-1 staining of lymphatic vessels. Recent evidence has indicated that immune cells, such as macrophages and dendritic cells, also express LYVE-1[44-46], which would affect precise cell identification using 3DTC. Due to the fact that different renal injuries cause distinct immune infiltration and dynamics[39], we suggest investigators take advantage of the ability to co-stain sections for multiple specific cell surface markers to confidently distinguish immune cells from lymphatic vasculature.

Furthermore, limitations to 3DTC exist, as analysis is performed on fixed tissue in an *ex vivo* model, which perturbs intrinsic physiological and pathophysiological processes, including cellular redox status, metabolism, and ontogeny. Investigators can more precisely interrogate these processes using the ProxTom mice coupled to other techniques, such as two photon intravital imaging[47].

In summary, we have validated a technique to comprehensively study renal LA post-AKI. With the use of the ProxTom mice with highly visible red fluorescent lymphatic vessels, we demonstrate that 3DTC can be used to detect and image changes in lymphatic expansion after AKI for quantification and spatial studies. 3DTC is a robust tool that can be used to study LA without these mice as well, as we demonstrated its use with LYVE-1 marker staining. The ProxTom mice are therefore an important tool for renal lymphatic research and hold promise for further elucidating lymphatic function in the kidney.

Supplementary Material

Refer to Web version on PubMed Central for supplementary material.

Acknowledgments

This work was supported by VA Merit Award (1l01 BX004047 to AA), Indiana O'Brien Center for Advanced Microscopic Analysis (P30 DK079312 to TME-A), National Institute of Diabetes and Digestive and Kidney Diseases grant (T32 DK007545 to LMB), and the core resource of the UAB-UCSD O'Brien Center for AKI Research (NIH grant P30-DK-079337 to AA). We appreciate the surgical expertise of Zhengqin Yang and Yanlin Jiang.

Funding

This work was supported by VA Merit Award (1l01 BX004047 to AA), Indiana O'Brien Center for Advanced Microscopic Analysis (P30 DK079312 to TME-A), National Institute of Diabetes and Digestive and Kidney Diseases grant (T32 DK007545 to LMB), and the core resource of the UAB-UCSD O'Brien Center for AKI Research (NIH grant P30-DK-079337 to AA).

References

1. Zarjou Aet al.Dynamic signature of lymphangiogenesis during acute kidney injury and chronic kidney disease. Lab Invest99, 1376–1388 (2019). [PubMed: 31019289]
2. Bui K & Hong Y-K Ras Pathways on Prox1 and Lymphangiogenesis: Insights for Therapeutics. Front Cardiovasc Med 7, 597374 (2020). [PubMed: 33263009]
3. Tammela T & Alitalo K Lymphangiogenesis: Molecular mechanisms and future promise. Cell 140, 460–476 (2010). [PubMed: 20178740]
4. Frueh FSet al.A potential role of lymphangiogenesis for peripheral nerve injury and regeneration. Med Hypotheses135, 109470 (2020). [PubMed: 31734377]
5. Luo Det al.Natural product celastrol suppressed macrophage M1 polarization against inflammation in diet-induced obese mice via regulating Nrf2/HO-1, MAP kinase and NF-kappaB pathways. Aging9, 2069–2082 (2017). [PubMed: 29040966]
6. Hasegawa Set al.Vascular endothelial growth factor-C ameliorates renal interstitial fibrosis through lymphangiogenesis in mouse unilateral ureteral obstruction. Lab Invest97, 1439–1452 (2017). [PubMed: 29083411]
7. Nakamoto Set al.Lymphangiogenesis and accumulation of reparative macrophages contribute to liver repair after hepatic ischemia-reperfusion injury. Angiogenesis23, 395–410 (2020). [PubMed: 32162023]
8. Ny Aet al.Role of VEGF-D and VEGFR-3 in developmental lymphangiogenesis, a chemicogenetic study in Xenopus tadpoles. Blood112, 1740–1749 (2008). [PubMed: 18474726]
9. Shimizu Yet al.Impact of Lymphangiogenesis on Cardiac Remodeling After Ischemia and Reperfusion Injury. J Am Heart Assoc7, e009565 (2018). [PubMed: 30371303]
10. Natale G, Bocci G & Ribatti D Scholars and scientists in the history of the lymphatic system. J Anat 231, 417–429 (2017). [PubMed: 28614587]
11. Crivellato E, Travan L & Ribatti D The Hippocratic treatise 'On glands': the first document on lymphoid tissue and lymph nodes. Leukemia 21, 591–592 (2007). [PubMed: 17375122]
12. Jeltsch Met al.Hyperplasia of lymphatic vessels in VEGF-C transgenic mice. Science276, 1423–1425 (1997). [PubMed: 9162011]
13. Alitalo K, Tammela T & Petrova TV Lymphangiogenesis in development and human disease. Nature 438, 946–953 (2005). [PubMed: 16355212]
14. Russell PS, Hong J, Windsor JA, Itkin M & Phillips ARJ Renal Lymphatics: Anatomy, Physiology, and Clinical Implications. Front Physiol 10, 251 (2019). [PubMed: 30923503]
15. Tanabe K, Wada J & Sato Y Targeting angiogenesis and lymphangiogenesis in kidney disease. Nat Rev Nephrol 16, 289–303 (2020). [PubMed: 32144398]
16. Pei Get al.Lymphangiogenesis in kidney and lymph node mediates renal inflammation and fibrosis. Sci Adv5, eaaw5075 (2019). [PubMed: 31249871]
17. Suzuki Yet al.Transforming growth factor-beta induces vascular endothelial growth factor-C expression leading to lymphangiogenesis in rat unilateral ureteral obstruction. Kidney Int81, 865–879 (2012). [PubMed: 22258325]
18. Truman LAet al.ProxTom lymphatic vessel reporter mice reveal Prox1 expression in the adrenal medulla, megakaryocytes, and platelets. Am J Pathol180, 1715–1725 (2012). [PubMed: 22310467]
19. Winfree Set al.Quantitative Three-Dimensional Tissue Cytometry to Study Kidney Tissue and Resident Immune Cells. J Am Soc Nephrol28, 2108–2118 (2017). [PubMed: 28154201]
20. Winfree Set al.Large-scale 3-dimensional quantitative imaging of tissues: state-of-the-art and translational implications. Transl Res189, 1–12 (2017). [PubMed: 28784428]
21. Winfree Set al.Quantitative Large-Scale Three-Dimensional Imaging of Human Kidney Biopsies: A Bridge to Precision Medicine in Kidney Disease. Nephron140, 134–139 (2018). [PubMed: 29870980]
22. El-Achkar TMet al.A Multimodal and Integrated Approach to Interrogate Human Kidney Biopsies with Rigor and Reproducibility: Guidelines from the Kidney Precision Medicine Project. Physiol Genomics53, 1–11 (2020). [PubMed: 33197228]

23. Lever JMet al.Resident macrophages reprogram toward a developmental state after acute kidney injury. JCI Insight4, e125503 (2019).
24. El-Achkar TMet al.Tamm-Horsfall protein translocates to the basolateral domain of thick ascending limbs, interstitium, and circulation during recovery from acute kidney injury. Am J Physiol Renal Physiol304, F1066–1075 (2013). [PubMed: 23389456]
25. Ferkowicz MJet al.Large-scale, three-dimensional tissue cytometry of the human kidney: a complete and accessible pipeline. Lab Invest10.1038/s41374-020-00518-w (2021).
26. LaFavers KAet al.Circulating uromodulin inhibits systemic oxidative stress by inactivating the TRPM2 channel. Sci Transl Med11, 512:eaw3639 (2019).
27. Royer LAet al.ClearVolume: open-source live 3D visualization for light-sheet microscopy. Nat Methods12, 480–481 (2015). [PubMed: 26020498]
28. Basile DP, Anderson MD & Sutton TA Pathophysiology of acute kidney injury. Compr Physiol 2, 1303–1353 (2012). [PubMed: 23798302]
29. Pallet N, Thervet E & Timsit MO Angiogenic response following renal ischemia reperfusion injury: new players. Prog Urol 24, S20–S25 (2014). [PubMed: 24950928]
30. Kenig-Kozlovsky Yet al.Ascending Vasa Recta Are Angiopoietin/Tie2-Dependent Lymphatic-Like Vessels. J Am Soc Nephrol29, 1097–1107 (2018). [PubMed: 29237738]
31. Randi AM, Smith KE & Castaman G von Willebrand factor regulation of blood vessel formation. Blood 132, 132–140 (2018). [PubMed: 29866817]
32. Fraser JR, Kimpton WG, Laurent TC, Cahill RN & Vakakis N Uptake and degradation of hyaluronan in lymphatic tissue. Biochem J 256, 153–158 (1988). [PubMed: 3223897]
33. Oliver GLymphatic vasculature development. Nat Rev Immunol4, 35–45 (2004). [PubMed: 14704766]
34. Wigle JTet al.An essential role for Prox1 in the induction of the lymphatic endothelial cell phenotype. EMBO J21, 1505–1513 (2002). [PubMed: 11927535]
35. Jafree DJ & Long DA Beyond a Passive Conduit: Implications of Lymphatic Biology for Kidney Diseases. J Amer Soc Nephrol 31, 1178–1190 (2020). [PubMed: 32295825]
36. McIntosh GH & Morris B The lymphatics of the kidney and the formation of renal lymph. J Physiol 214, 365–376 (1971). [PubMed: 5580858]
37. Schwager S & Detmar M Inflammation and Lymphatic Function. Front Immunol 10, 308 (2019). [PubMed: 30863410]
38. Maruyama Ket al.Inflammation-induced lymphangiogenesis in the cornea arises from CD11b-positive macrophages. J Clin Invest115, 2363–2372 (2005). [PubMed: 16138190]
39. Black LMet al.Divergent effects of AKI to CKD models on inflammation and fibrosis. Am J Physiol Renal Physiol315, F1107–F1118 (2018). [PubMed: 29897282]
40. Corliss BA, Azimi MS, Munson JM, Peirce SM & Murfee WL Macrophages: An Inflammatory Link Between Angiogenesis and Lymphangiogenesis. Microcirculation 23, 95–121 (2016). [PubMed: 26614117]
41. Cursiefen Cet al.VEGF-A stimulates lymphangiogenesis and hemangiogenesis in inflammatory neovascularization via macrophage recruitment. J Clin Invest113, 1040–1050 (2004). [PubMed: 15057311]
42. Guo YCet al.Macrophages Regulate Unilateral Ureteral Obstruction-Induced Renal Lymphangiogenesis through C-C Motif Chemokine Receptor 2-Dependent Phosphatidylinositol 3-Kinase-AKT-Mechanistic Target of Rapamycin Signaling and Hypoxia-Inducible Factor-1alpha/Vascular Endothelial Growth Factor-C Expression. The Am J Pathol187, 1736–1749 (2017). [PubMed: 28627412]
43. Ran S & Montgomery KE Macrophage-mediated lymphangiogenesis: the emerging role of macrophages as lymphatic endothelial progenitors. Cancers (Basel) 4, 618–657 (2012). [PubMed: 22946011]
44. Brezovakova V, & Jadhav S. Identification of Lyve-1 positive macrophages as resident cells in meninges of rats. J Comp Neurol 528, 2021–2032 (2020). [PubMed: 32003471]

45. Lim HY, Lim SY, Tan CK, Thiam CH, Goh CC, Carbajo D, et al.Hyaluronan Receptor LYVE-1-Expressing Macrophages Maintain Arterial Tone through Hyaluronan-Mediated Regulation of Smooth Muscle Cell Collagen. Immunity49, 326–41.e7 (2018). [PubMed: 30054204]

46. Rinaldi E, & Baggi F. LYVE-1 is 'on stage' now: an emerging player in dendritic cell docking to lymphatic endothelial cells. Cell Mol Immunol. 15, 663–5 (2018). [PubMed: 29176746]

47. Hato T, Winfree S, Day R, Sandoval RM, Molitoris BA, Yoder MC, et al.Two-Photon Intravital Fluorescence Lifetime Imaging of the Kidney Reveals Cell-Type Specific Metabolic Signatures. J Amer Nephrol28, 2420–2430 (2017).

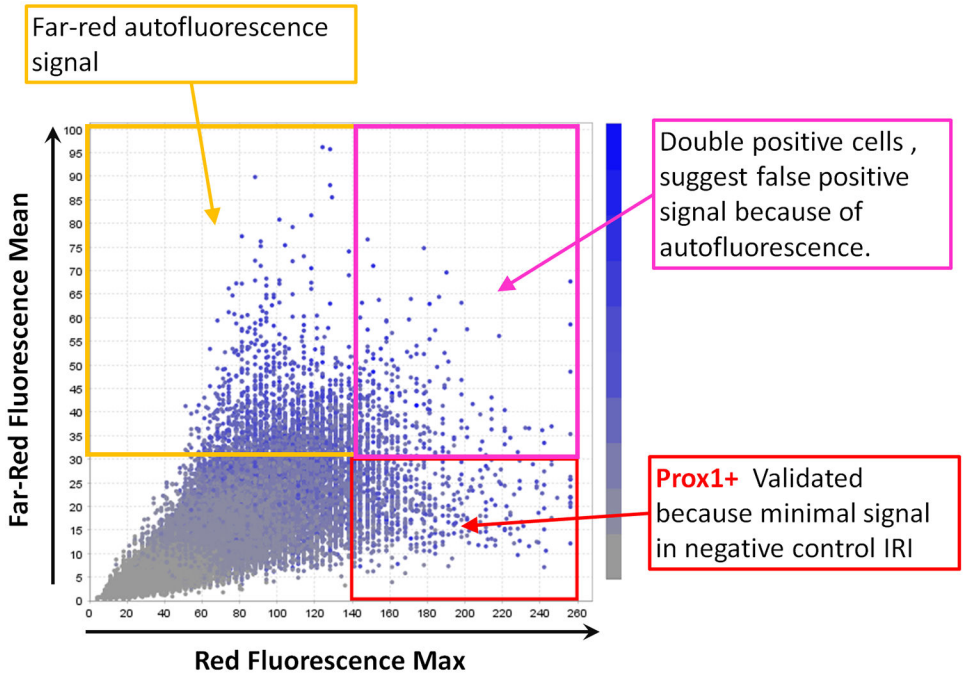

Figure 1. VTEA analysis methods to parse autofluorescence (AF) post-AKI.
Gating strategy used to survey tdTomato positive cells and separate the tdTomato fluorescence from AF signal.

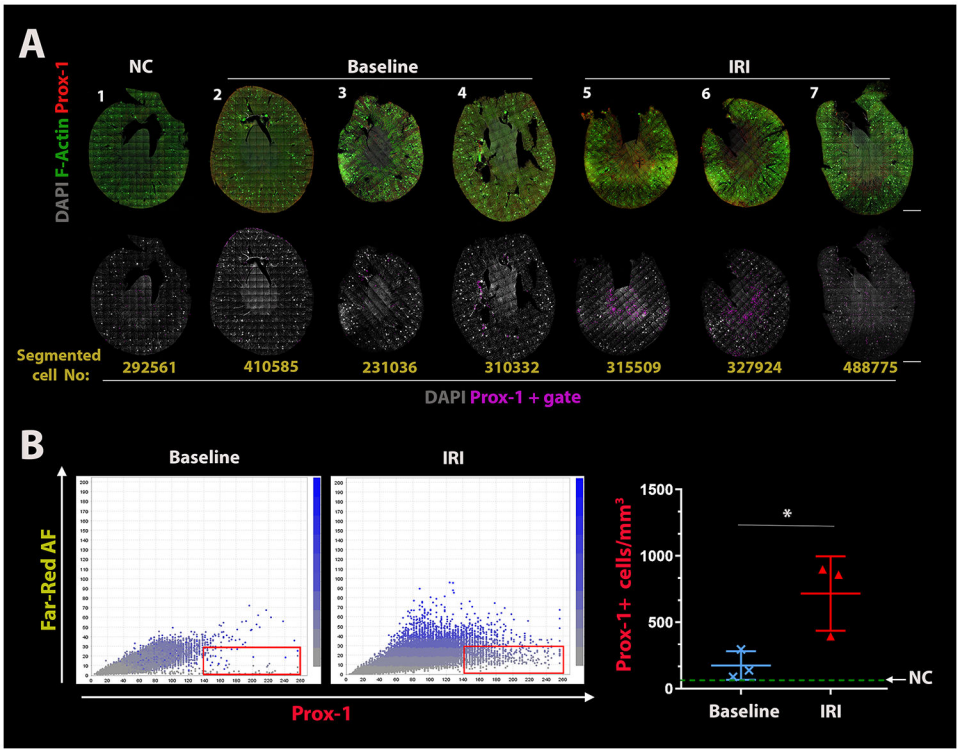

Figure 2: Large-scale 3D imaging and cytometry analysis of Prox-1 mouse kidneys suggests lymphatic expansion following IRI.

A: Maximum projection images of samples 1-7 (top row shows fluorescence signal from 3 channels, bottom shows the distribution of Prox-1+ gated cells using nuclear overlays in magenta). The number of segmented cells in each section is displayed at the bottom of each sample in yellow. *B:* Representative scatter plots and gates to identify Prox-1+ cells in baseline and IRI samples, and a summary plot from all samples is shown on the far right. Scale bars = 1mm. (NC=negative control). The brightness/contrast was enhanced for clarity using Adobe Photoshop.

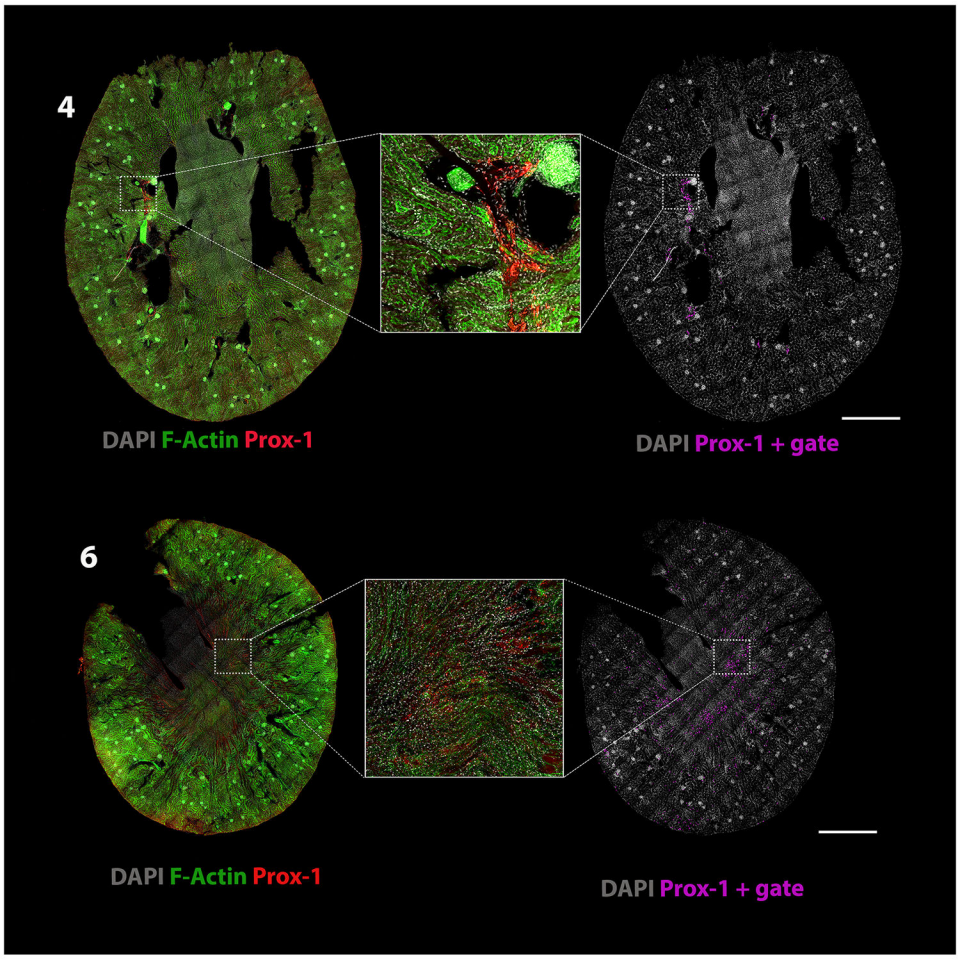

Figure 3: Distribution of Prox-1+ cells shifts from hilum to the inner medulla post-IRI.
Shown are enlarged maximum projection images of specimen 4 (top, Baseline), with a further enlarged image from the boxed area showing Prox-1+ cells at baseline. On the bottom, enlarged images of specimen 6 (IRI), showing the increased density of Prox-1 + cells in the inner stripe of the outer medulla. Scale bars = 1 mm. The brightness/contrast of the image was uniformly enhanced using Adobe Photoshop for clarity.

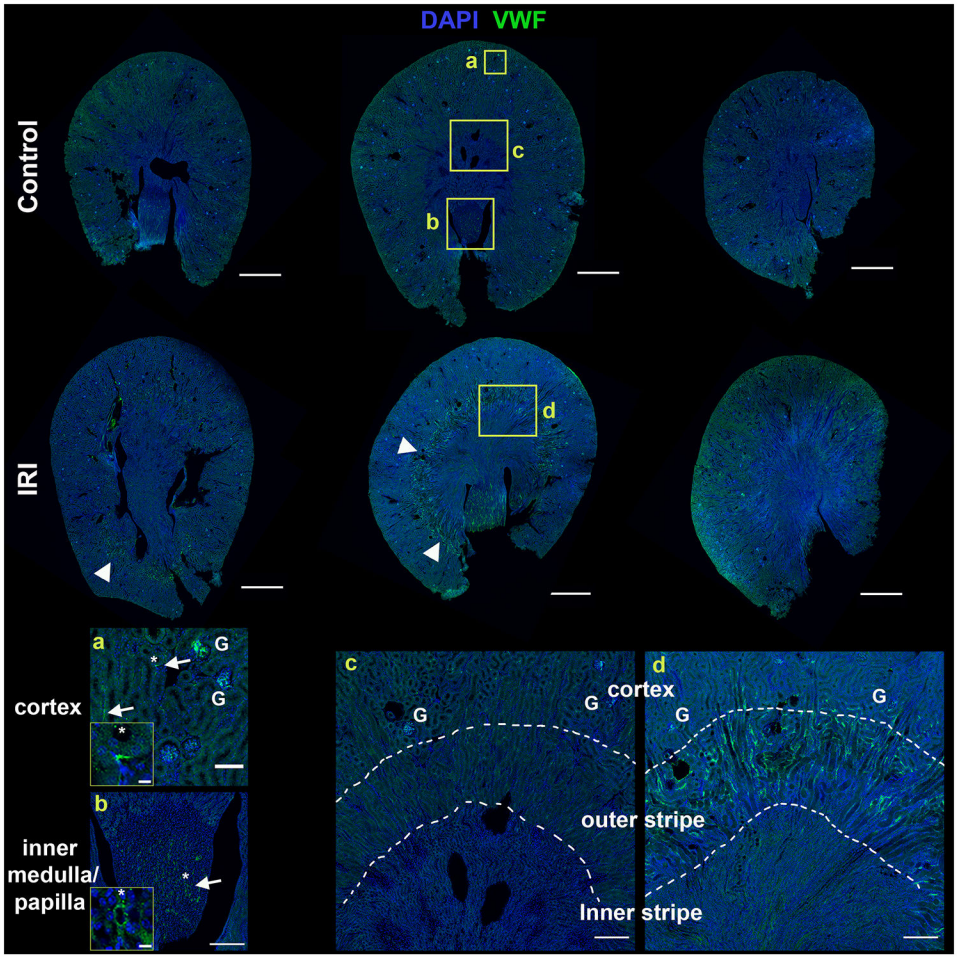

Figure 4: Endothelial cell changes post-injury are distinct from those observed for lymphatics.

Large scale imaging of kidney sections from control and IRI kidney sections stained for Von Willebrand Factor (VWF) to label endothelial cells (n=3 per group). *Top row:* In control samples, VWF staining was predominately observed in the cortex [*Inset a:* Glomeruli (G) and peritubular capillaries (Arrows)] and in the deep inner medulla and papilla (*Inset b:* Likely vasa recta and capillaries). High magnification images are included within insets *a* and *b* to show enlarged images of areas marked by *****. *Middle row:* After IRI, there was a variable increase in VWF signal (arrowheads), observed predominantly in part of the outer stripe of the outer medulla (outlined by dotted lines) and the cortico-medullary junction (Inset *d* from IRI compared to Inset *c* from control). Scale bars in the first 2 rows = 1 mm. Scale bar in *a* is 100 μm. Scale bars in *b, c,* and *d* are 250 μm. High magnification images within insets *a* and *b* are 10 μm. These changes are distinct from what we observed for Prox-1+ cells after injury.

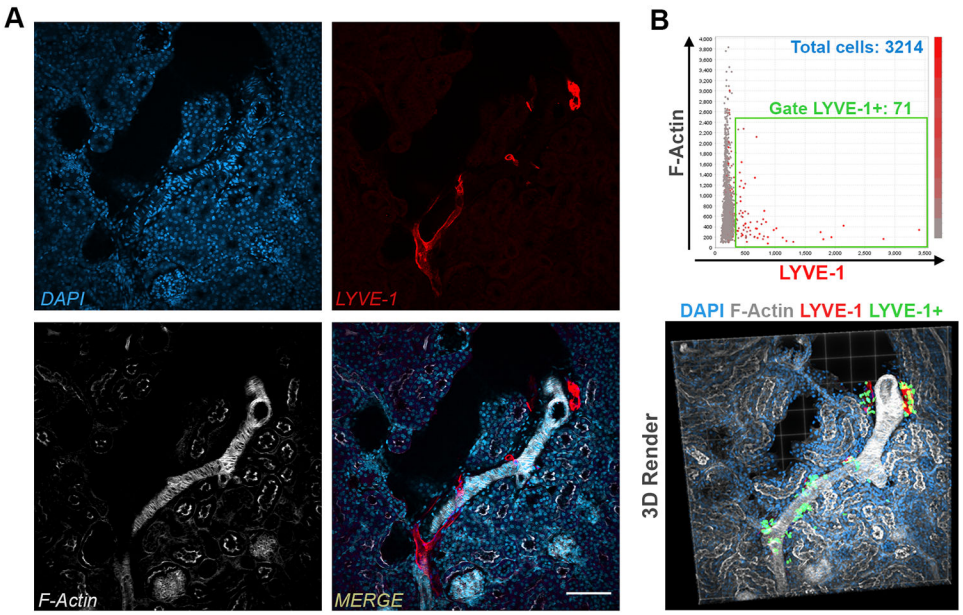

Figure 5: 3D imaging and tissue cytometry of LYVE-1.

A: An optical section from a single 3D volume obtained using confocal imaging of a control mouse imaged after staining for LYVE-1, DAPI and F-actin. **B:** Tissue cytometry performed on this small volume using VTEA, showing gating for LYVE-1 cells (top) and visualization of the gated cells using 3D rendering with ClearVolume.

Table 1.

Results from all the samples in a tabular form, with the total number of Prox-1+ cells identified in each section, the percentage out of the total number of segmented cells, and the density of Prox1+ cells in each sample, calculated by dividing the number of Prox-1 cells by the actual volume imaged and segmented by VTEA.

Condition	Genotype	Prox-1$^+$ Cells	Total Cells	Prox-1$^+$ Cell %	Prox-1$^+$ Density (cells/mm^3)
IRI	Negative	69	292561	0.024	68.10
BL	Positive	121	410585	0.030	89.28
BL	Positive	77	231036	0.033	138.55
BL	Positive	270	310332	0.087	295.28
IRI	Positive	720	315509	0.228	858.58
IRI	Positive	846	327924	0.258	898.62
IRI	Positive	435	488775	0.0890	394.48